

## Highlights

### **AVSim - Realistic Simulation Framework for Airborne and Vector-Borne Disease Dynamics**

Pandula Thennakoon, Mario De Silva, M. Mahesha Viduranga, Sashini Liyanage, Roshan Godaliyadda, Mervyn Parakrama Ekanayake, Vijitha Herath, Anuruddhika Rathnayake, Ganga Thilakarathne, Janaka Ekanayake, Samath Dharmarathne

- Human mobility modeling using machine learning and probabilistic models.
- Unveiling hidden behavioral patterns via unsupervised clustering and graph theory.
- Agent-based model with realistic scalable environments and transportation systems.
- Simulates airborne and vector-borne disease spread dynamics.
- Provides micro-level insights for public health planning and response.

# AVSim - Realistic Simulation Framework for Airborne and Vector-Borne Disease Dynamics

Pandula Thennakoon<sup>a</sup>, Mario De Silva<sup>a</sup>, M. Mahesha Viduranga<sup>a,b</sup>, Sashini Liyanage<sup>b,c,\*</sup>, Roshan Godaliyadda<sup>a,b</sup>, Mervyn Parakrama Ekanayake<sup>a,b</sup>, Vijitha Herath<sup>a,b</sup>, Anuruddhika Rathnayake<sup>d</sup>, Ganga Thilakarathne<sup>e</sup>, Janaka Ekanayake<sup>a,b</sup> and Samath Dharmarathne<sup>d</sup>

<sup>a</sup>Department of Electrical and Electronic Engineering, University of Peradeniya, Sri Lanka

<sup>b</sup>Multidisciplinary AI Research Center, University of Peradeniya, Sri Lanka

<sup>c</sup>Department of Computer Engineering, University of Peradeniya, Sri Lanka

<sup>d</sup>Faculty of Medicine, University of Peradeniya, Peradeniya, Sri Lanka

<sup>e</sup>Institute of Policy Studies, Colombo, Sri Lanka

## ARTICLE INFO

### Keywords:

Agent-based model (ABM)  
airborne diseases  
vector-borne diseases  
epidemiology  
public health intervention

## ABSTRACT

The COVID-19 pandemic underscored the critical need for rapid epidemic trend identification and effective intervention strategies to mitigate disease progression and its socio-economic impact. Concurrent with emerging threats, endemic diseases like dengue continue to strain healthcare systems, particularly in populous, economically challenged nations. This paper introduces AVSim (Airborne and Vectorborne Simulator), an agent-based model designed to provide granular insights for optimizing resource allocation within existing healthcare management frameworks. AVSim leverages realistic human mobility and behavioral patterns to simulate disease propagation within a detailed, scalable environment encompassing homes, schools, hospitals, and commercial venues. Human movement is modeled based on occupational and behavioral patterns, including age-specific activities. The simulator incorporates age- and environment-specific disease outcomes, host-host and host-vector interactions, and multiple disease stages, including mild, severe, and critical phases. Immunity, quarantine, and hospitalization are also modeled. Furthermore, AVSim supports tracing the path of disease spread, providing micro-level insights into transmission dynamics. Implemented in Python, AVSim offers flexibility and extensibility, enabling users to create highly customized scenarios for airborne and vector-borne disease modeling. Case studies demonstrating AVSim's application to COVID-19 and dengue illustrate its potential for generating actionable epidemic insights, thereby enhancing public health planning and response.

## 1. Introduction


The COVID-19 pandemic lasted over three years, resulting in more than 700 million cases and claiming over 7 million lives [1]. This crisis highlighted the critical importance of timely interventions and coordinated efforts by individuals, healthcare systems, and governments to control disease outbreaks and prevent them from escalating into pandemics. Beyond COVID-19, vector-borne diseases, transmitted by living organisms that carry infectious pathogens between humans or from animals to humans, pose a significant public health challenge, causing over 700,000 deaths annually. For instance, In 2024, the World Health Organization (WHO) estimated approximately 249 million global cases of malaria and 100–400 million cases of dengue each year [2]. Many vector-borne and airborne diseases, including those similar to COVID-19, are preventable through protective measures and effective community mobilization. These preventable diseases underscore the need for continued vigilance, innovative interventions, and global collaboration to mitigate the risk of future outbreaks and safeguard public health.

Numerous methods have been employed to model disease spread and uncover patterns to better understand disease

propagation so that effective disease control strategies could be adopted efficiently while minimizing the net burden. These models can be broadly classified into two categories: compartment models and agent-based models (ABMs). Compartment models are relatively simple and computationally efficient. Within the compartmental modeling framework, the Susceptible-Exposed-Infectious-Recovered (SEIR) model has been widely used to study epidemics and pandemics [3]. These models classify individuals by their disease status and use differential equations to describe transitions between these states. Although they can give an overview of the disease's spread, they fail to capture many important details. Despite this, numerous attempts exist to model disease spread with such compartment models. Shaobo He et al. [4] used an SEIR compartment model based on the data from Hubei province (China) to show the evolution of the COVID-19 epidemic. Jonas Dehning et al. [5] focused on COVID-19 spread in Germany and used a SIR model to quantify the effect of interventions. Giulia Giordano et al. [6] proposed a new extended compartment model, SIDARTHE (Susceptible-Infected-Diagnosed-Ailing-Recognized-Threatened-Healed-Extinct), that predicts the course of the epidemic to help plan an effective control strategy.

Agent-based models, on the other hand, are more complex and able to deliver micro-level details about each agent

\*Corresponding author

 sashinil@eng.pdn.ac.lk (S. Liyanage)

ORCID(s):

in the simulation. They have the capability to model interactions between agents or entities in a defined environment. Each agent follows a set of well-defined rules, allowing ABMs to capture emergent behaviors that arise from these interactions. This makes them particularly useful for modeling complex systems in fields like epidemiology [7, 8], urban planning [9], ecology [10], and molecular-level biological [11, 12] systems. The ability to incorporate fine-grained details enhances decision-making, especially for policymakers seeking accurate predictions.

The use of ABMs in epidemiology has grown significantly during the COVID-19 pandemic. Models like Covasim [7], PDSIM [13], and OpenABM [8] have been widely used to analyze disease dynamics and inform public health responses. Some benchmark ABMs are mentioned and compared with our proposed ABM in Table 1.

Additionally, there has been increasing research on the dynamic analysis of vector-borne diseases. One notable approach by Carrie Manore et al. [14] employs an ABM to analyze the propagation of mosquito-borne diseases. This study introduces the network-patch method, utilizing differential equations to model mosquito density. Similarly, Imran Mahmood et al. [15] use an ABM to compute vector density based on the reproductive behavior of vectors. However, their model does not incorporate realistic movement patterns, limiting its ability to provide real-world insights. Another study applied a fuzzy modeling approach to develop an epidemic model for mosquito-borne diseases [16].

A comprehensive modeling and analysis tool, such as ABM or otherwise, helps to be better prepared for an epidemic situation. For example, during the initial stages of the COVID pandemic, there were many unknowns and uncertainties resulting in confusion, stressing of healthcare resources, as well as burdening the public excessively due to the control strategies. Many of the initial responses involved in reactive measures such as contact tracing and mass-scale quarantining and lock-downs. A comprehensive computational model would, on the other hand, complement the existing diverse healthcare systems and practices of countries and regions by making it possible to "play out" different scenarios using the best of data and knowledge available and/or learned assumptions on what may happen under different cases. Armed with all these possible outcomes, healthcare resources could be targeted effectively and efficiently so that maximum outcomes could be attained.

Effective intervention and prevention strategies in epidemiology require modeling disease spread under realistic conditions. Human mobility, behavioral patterns, and public modes of transportation significantly influence the speed and extent of pathogen transmission [13]. Different behaviors and transport modes affect disease spread in varied ways. However, many models either overlook these variations [17, 18] or rely on oversimplified assumptions, such as treating transportation as random interactions aggregated with activities like shopping or social events [7, 19], failing to reflect real-world complexities.

To address the limitations of existing methods, we propose an agent-based model for vector-borne and airborne diseases, named AVSim, that uses real-world data and accounts for real-world conditions. Our framework learns and models different human mobility and behavioral patterns, simulating agents based on occupation and behavior at a granular level. It incorporates a realistic environment and public transportation model to simulate disease spread. The proposed model is customizable and extendable, offering a flexible framework adaptable to various diseases and transmission modes, thus enhancing its applicability to emerging public health challenges. A preliminary version of this work was presented in [20, 21]. In this article, we expand on our previous findings by introducing additional experiments, deeper analysis, and improved methodologies. We further demonstrate the framework's use in simulating COVID-19 and dengue propagation through an extended SEIR model within an ABM.

## 2. Material and methods

The proposed AVSim consisted of two major stages. The first stage was the data generation stage, where human mobility and behavioral patterns were identified and generated using real-world data. This sets the foundation for the second stage of AVSim: the simulation of the ABM. As shown in Fig. 1, the ABM simulation stage comprised four main components: the environment, vector patch, transportation, and agent generation. However, for simulating vector-borne diseases, only the environment, vector patch, and agent generation components were used, as transportation had no significant impact on disease spread. Conversely, for airborne diseases, only the environment, transportation, and agent generation components were utilized. Each of these stages will be explained in detail in the following sections.

### 2.1. Modeling human behaviour

To accurately model disease spread in a human population, it was essential to replicate realistic human motion patterns within the simulation environment. In the context of human motion, various factors affected:

- Time-dependent location visits: Individuals visit specific locations based on the time of day.
- Duration of stay: The length of time spent at a location varies depending on the time of day and the nature of the location.
- Profession-dependent behavior: The types of locations visited and the associated durations differ based on individuals' professions.

To address these factors, In the first stage of AVSim, we proposed a method for generating realistic human motion patterns using real-world GPS data. This approach enabled us to delve deeper into human mobility and behavioral dynamics, uncovering insights that were not immediately apparent. The following subsections outline the data acquisition process and the methods used for pattern recognition.

**Table 1**

Comparison of disease simulators found in the literature with ours.

Simulation Method	Simulator	Realistic Human Motion	Use of real mobility data	Realistic Environment	Transport System	Testing Protocol	Vaccination Strategy	Containment Strategy	Hygiene Protocol	Tracing Path of Disease Spread	User-Friendly Interface	Detailed agent modeling	Environmental Factors	Simulation
Vector-borne Diseases	Network-patch methodology for adapting disease models [14]	✓												✓
	Agent-Based Simulation of Dengue Fever Spread [15]			✓		✓					✓	✓	✓	✓
	Climate-based dengue model in Semarang, Indonesia [22]			✓		✓						✓	✓	✓
	ABM for vaccine efficacy's influence on public health projections [23]	✓		✓		✓	✓		✓			✓	✓	✓
	ABM driven by rainfall to study chikungunya outbreak [24]	✓		✓		✓			✓	✓	✓	✓	✓	✓
	<b>AVSim (Our Approach)</b>	✓	✓	✓		✓		✓	✓	✓	✓	✓	✓	✓
Air-borne Diseases	Covasim [7]					✓	✓	✓	✓	✓	✓			
	OpenABM-Covid19 [8]					✓	✓	✓	✓	✓	✓			
	PDSIM [13]	✓			✓	✓	✓	✓	✓	✓	✓	✓		
	A particle-based COVID-19 simulator [25]					✓			✓	✓				
	Simulator of interventions for COVID-19 [26]					✓		✓	✓	✓				
	People meet people [27]					✓		✓	✓	✓				
	COVID-town [28]					✓	✓	✓	✓	✓				
	An Agent-based modeling of COVID-19 [29]					✓		✓	✓	✓				
	Social bubble vanpooling (SBV) [30]				✓	✓		✓	✓	✓				
	<b>AVSim (Our Approach)</b>	✓	✓	✓	✓	✓	✓	✓	✓	✓	✓	✓	✓	✓

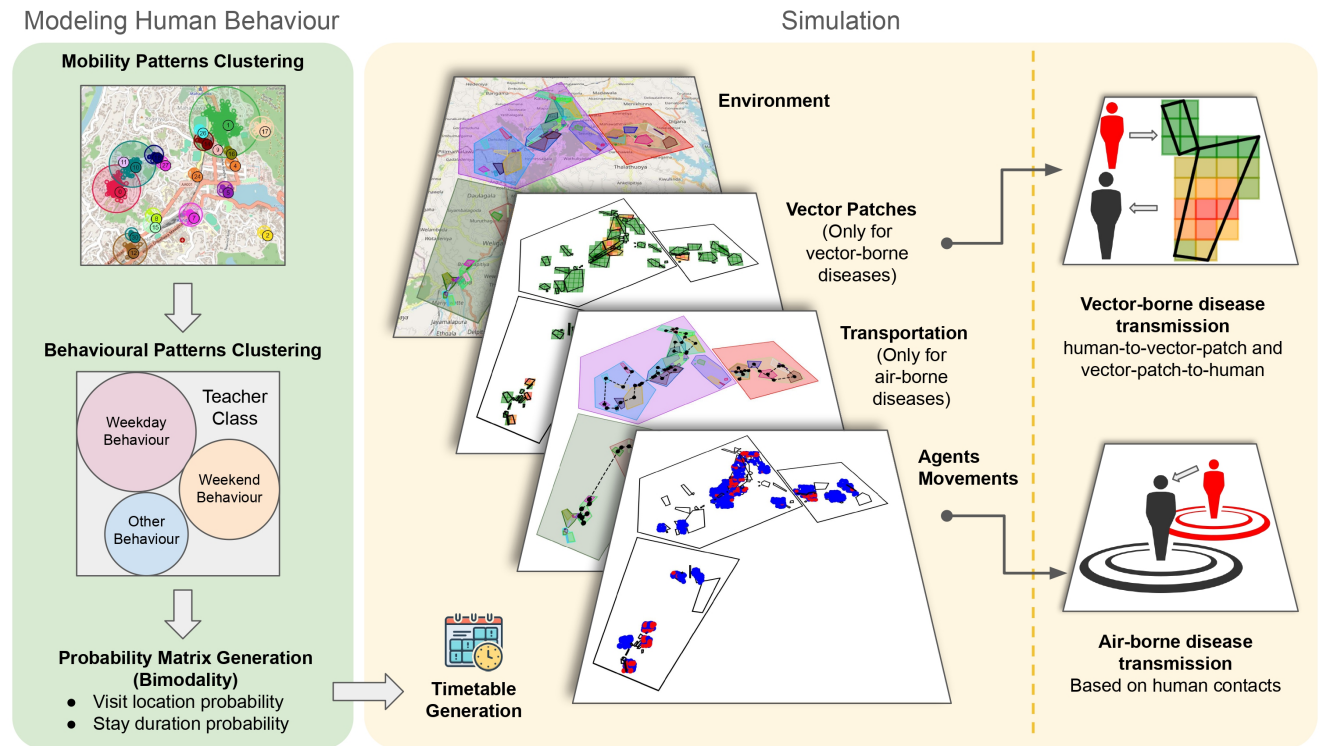


**Figure 1:** Overview of the proposed agent-based model structure, illustrating the key components: environment, vector-patch, transportation, agent simulation, and the two disease transmission models: vector-borne and airborne.

### 2.1.1. Tracking human movement and data acquisition

The first step in modeling human motion was gathering a large and diverse dataset of real-world movement patterns. To achieve this, GPS tracking of human agents was conducted using a smartphone application. The dataset was sourced from 100 voluntary participants residing in

the Kandy district of Sri Lanka, each representing one of 13 distinct professions. The participants' GPS coordinates, altitude, and timestamps were recorded at 5-minute intervals over 21 days. This duration was chosen as the optimal time frame for capturing representative mobility patterns while remaining manageable for participants. A longer duration



could have led to participant fatigue or reduced engagement, affecting data quality. To enhance diversity and fairness, participants within a single profession were carefully selected to reflect varying factors such as age, gender, and the relative distance between their workplace and residence.

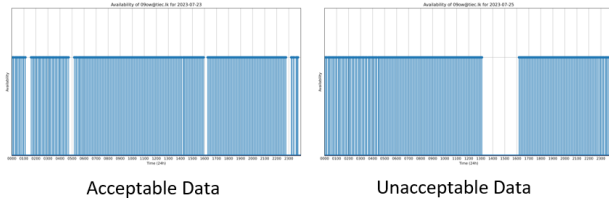


**Figure 2:** An example of accepted and unaccepted patterns based on daily data availability.

Before enrollment, all participants were well informed about the scope of the data being collected and its intended use. Informed verbal and written consent were obtained from each participant, with students requiring additional consent from a parent or guardian and their educational institution. Upon consent, participants were provided with the smartphone application and instructed to keep their smartphones active and within reach throughout the study. Data privacy and confidentiality were maintained at all stages, and all data was anonymized.

**Ethical approval:** The ethical clearance for this study was obtained from the Ethical Review Committee, Faculty of Arts, University of Peradeniya, Sri Lanka, (ARTS/ERC/2021/01 and 18 September 2021) with the support of the Department of Sociology. Administrative clearance was obtained by the Ministry of Home Affairs of Sri Lanka, relevant Divisional Secretariate (DS) offices, and relevant Grama Niladari (GN) offices.

To ensure data quality, daily datasets were reviewed for completeness, and 21 complete daily datasets were required per participant. A day was considered complete if at least 80% of the expected 288 data points (recorded every 5 minutes) were present and evenly distributed throughout the day, minimizing gaps in coverage. Days with more than 20% missing data (57 data points) or significant periods of consecutive data loss were excluded. As a result, data collection for a participant typically extended beyond 21 days to ensure 21 days of complete data. Fig. 2 shows an example of accepted and discarded data based on its availability throughout the day.

### 2.1.2. Human mobility patterns identification

The GPS data was recorded in the time and coordinate domain (longitude and latitude), making it specific to the geographical environment where it was collected, in this case, Kandy, Sri Lanka. However, human motion patterns are generally consistent across different geographical locations. For example, a teacher's typical working day will not depend on the geographical location. They will be at the resting place in the morning, leave for work, maybe visit some places in the evening, and return to the resting place

at the end of the day. To make the data applicable beyond the specific geographic context, we transformed it into a time and location domain that removes the dependency on physical coordinates. This transformation generalizes the data, enabling broader applicability and analysis of human motion patterns.

To identify the locations visited by each person, the GPS data for all participants over the 21 days was plotted on a map of Sri Lanka. Fig. 3 illustrates the raw GPS data when mapped geographically. The data reflects the places visited and the movements during transportation, such as commuting between locations.

When zooming in on these denser clusters, which occur at locations where the person pauses, additional sub-clusters emerge within them, revealing further granularity. Fig. 3

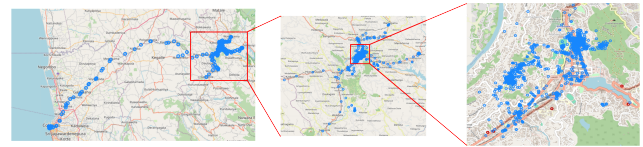


**Figure 3:** Hierarchical clustering of locations as we zoom into GPS data.

demonstrates this inherent pattern in human motion. This pattern highlights a hierarchical structure in the locations visited, with primary locations further divided into more specific destinations.

For this study, our primary interest lies in the denser clusters of GPS data, which indicate areas where participants spent more time, such as workplaces, homes, and other specific locations.

To identify these clusters, a clustering method needs to be deployed. In this study, we employed the Density-Based Spatial Clustering of Applications with Noise (DBSCAN), which produced effective results. DBSCAN is a popular density-based clustering algorithm known for detecting clusters of varying densities while being robust to noise. References [31] and [32] proved to be useful in implementing the DBSCAN algorithm. Unlike K-Means clustering and Gaussian Mixture Models, DBSCAN does not require the number of clusters to be specified in advance. Instead, it determines the number of clusters based on the data, which makes it well-suited for identifying clusters in GPS data. DBSCAN classifies points into three categories: core points, border points, and noise points. Core and border points form the clusters, while noise points are discarded. As a result, transportation-related data is treated as noise and removed from the analysis. The DBSCAN algorithm requires two initial parameters:

1. epsilon ( $\epsilon$ ) defines the maximum distance between two points in a cluster.
2. minPts, the minimum number of points required for a point to be considered a core point of a cluster.

To determine the most suitable values for these parameters, we experimented with different values of  $\epsilon$  and

minPts. Through an iterative process of testing and evaluating clustering performance, we found that setting  $\epsilon = 5$  and minPts = 10 produced the most meaningful and consistent clusters. These values effectively distinguished visited locations while minimizing noise, making them optimal for our specific application.

Since the primary goal was to convert time-coordinates domain data into the time-location domain, the next step involved identifying the numbered clusters as real-world locations. For this, commonly visited locations such as "Home," "School," and "Bank" were made into a list and grouped into broader categories like "Residential Zone," "Education Zone," and "Commercial and Financial Zone". Each cluster was then labeled based on these predefined locations and zones. For example, if a cluster represented an individual's

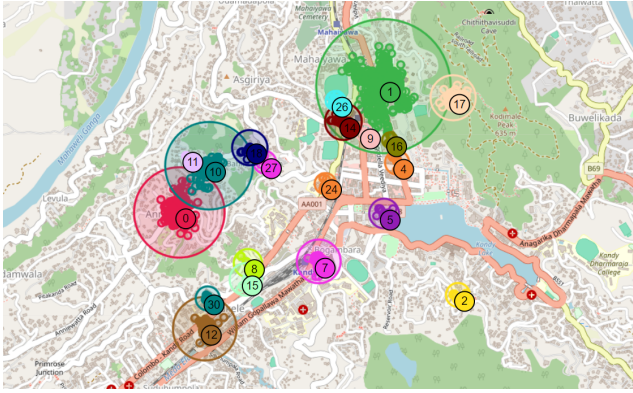


**Figure 4:** Clustering GPS data using DBSCAN algorithm.

home, it was labeled as "Home." Similarly, clusters corresponding to areas around the individual's neighborhood were labeled as "Residential Zone."

During this process, some clusters could not be mapped to identifiable real-world locations. This may have occurred for several reasons, such as GPS data drift, a phenomenon where the reported GPS position shifts over time despite the device being stationary, or network connectivity issues that affected the accuracy of location tracking. Additionally, even if the individual visited the area corresponding to a cluster, it might not match any meaningful location in the predefined list. These clusters were treated as outliers and excluded from the analysis.

The original dataset was recorded at a 5-minute resolution with some missing data points. However, the emulator (described in subsequent sections) operates at a 1-minute resolution. To bridge this gap, the data was reconstructed using Zero Order Hold (ZOH) reconstruction. This method was deemed sufficient because of several key factors. First, it was reasonable to assume that a person's location remained approximately constant within the 5-minute intervals between recorded points. Additionally, the dataset had been carefully preprocessed to ensure that missing data was minimal, allowing interpolation to address these gaps with negligible inaccuracies.

The reconstructed dataset with a 1-minute resolution is visualized in Fig. 5. It is important to note that transportation-related data points were excluded during the DBSCAN clustering process and are, therefore, not present in the final dataset. This dataset was used to model human movements in the proposed AVSim.

### 2.1.3. Human behavioural patterns identification

In this study, GPS data was collected from individuals belonging to various professional classes. This data was used to uncover the hidden structure of society based on occupation. Within each professional class, sub-professional class behaviors can be identified, as shown in Fig. 1.

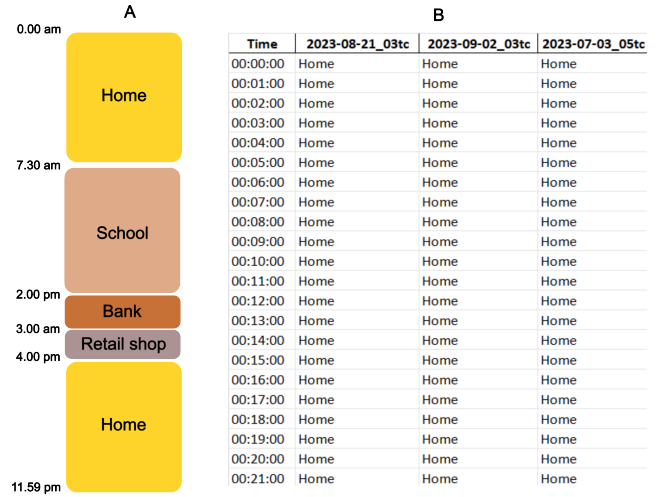


**Figure 5:** Final dataset: A visual representation of the trajectory of a teacher for a regular workday (A) and a part of the actual final dataset (B).

The Spectral Clustering method, which utilizes spectral graph theory [33], was employed to uncover hidden behavior patterns or sub-classes within each occupational class. Spectral clustering is an algorithm that considers the global structure of a dataset and determines the optimal number of clusters within it.

Although there is a lot of literature on spectral clustering within machine learning, the sources [34] and [35] proved to be of great value when applying spectral clustering to unlock hidden patterns in the dataset.

For the clustering process, locations needed to be encoded numerically. A 6-digit binary encoding was used, where the first three digits uniquely represent the zones, and the last three digits uniquely identify the locations within those zones, as defined in Section 2.1.2. This encoding ensured a clear separation between distinct locations, while locations within the same zone had less separation, reflecting their relative proximity or similarity. This compact numerical representation of locations facilitated effective clustering and produced acceptable results, as elaborated in Section 3.1.

Let us consider a day as a data point. Then we can represent our data set ( $X$ ) as,  $X = x_1, x_2, x_3, \dots, x_n$  and the notion of similarity between  $x_i$  and  $x_j$  as  $S_{ij} > 0$ .

To define similarity, we have chosen a Gaussian kernel, as shown below.

$$S_{i,j} = \begin{cases} \exp(-\frac{\|x_i - x_j\|^2}{2\sigma^2}) & i \neq j \\ \mu & i = j \end{cases} \quad (1)$$

Here, sigma is a scaling parameter that determines the closeness of data points to be considered a cluster. The other parameter  $\mu$  is a predefined value. In this study, it will be referred to as self-similarity, which will be in the range of [0,1].

The Gaussian kernel was selected because it will assign high similarity to close-by points, allowing them to cluster together and assign zero similarity to points far apart. This means that the number of clusters will depend on the sigma value, which is evident from the results.

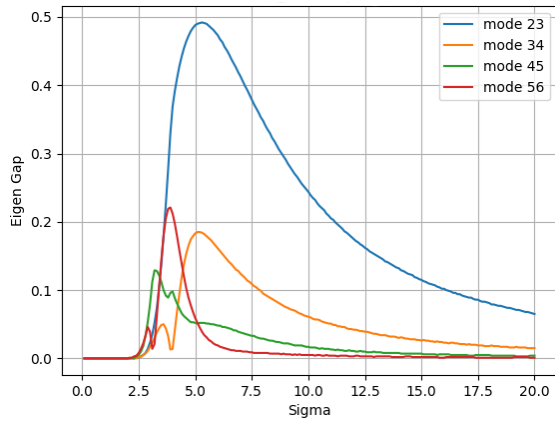


**Figure 6:** Sigma sweep for bank worker occupation class.

First, a similarity matrix (Adjacency matrix) was formulated as mentioned below.

$$A_{n,m} = \begin{pmatrix} S_{1,1} & S_{1,2} & \cdots & S_{1,n} \\ S_{2,1} & S_{2,2} & \cdots & S_{2,n} \\ \vdots & \vdots & \ddots & \vdots \\ S_{m,1} & S_{m,2} & \cdots & S_{m,n} \end{pmatrix} \quad (2)$$

Next, we created the degree matrix as,

$$D_{[i,j]} = \begin{cases} \sum_j A_{[i,j]} & i = j \\ \mu & otherwise. \end{cases} \quad (3)$$

Then, the symmetric normalized Laplacian was obtained,

$$L = I - D^{-1/2} A D^{-1/2}. \quad (4)$$

Thereafter, eigen decomposition was performed on the Laplacian matrix. The eigenvalues were then arranged in ascending order. The next procedure involved conducting a sigma sweep by plotting the eigen gaps between the sorted eigenvalues against sigma, as shown in Fig. 6. Note that mode  $xy$  corresponds to the eigen gap between  $x^{\text{th}}$  and  $y^{\text{th}}$  eigenvalues after sorting.

Using the aforementioned sigma sweep plot as a reference, the number of optimal clusters can be determined by applying the selection algorithm outlined below:

1. Largest Gap Value: The eigen gap with the highest value was considered as the prominent mode.
2. Selection of Dominant Sigma: Once the prominent mode is determined, the sigma value corresponding to the highest gap value for this mode is selected as the dominant sigma according to the selection algorithm [35].
3. Clustering Procedure: With the prominent mode and dominant sigma identified, clustering can be executed by following the steps described in [35].

When considering the sigma sweep for the bank worker class, as shown in Fig. 6, the prominent mode could be determined as 23, which would mean the behavior would be broken down into two significant clusters at the corresponding sigma value. Then the matrix,

$$X = [v_1, v_2, v_3, \dots, v_n] \in \mathbb{R}^{n \times n}, \quad (5)$$

can be formulated by stacking eigenvectors in columns. By treating each row of  $X$  as a point, the resulting points can be clustered into the desired number of groups using K-means clustering.

The above method was proven to be very successful in identifying hidden motion patterns within each profession class. These results were used to model human behavior, which will be discussed in the next section.

#### 2.1.4. Bimodality probability matrix generation

To model human motion, we employed a robust probabilistic approach capable of capturing complex movement dynamics, as introduced by Weligampola et al. [13]. This method enabled the generation of daily trajectories for agents within a predefined environment, taking into account the type of day (weekday or weekend) and the agent's profession.

The inspiration for adopting this method stemmed from observations of GPS trajectories. As previously observed, denser points in GPS data were the locations where people tended to stay for a longer time. It was further observed that human motion consists of pseudo-random visits to locations and a stay time associated with each location. These observations form the basis of the theory proposed by Weligampola et al. [13].

To model human movement, the theory introduces two probability matrices with size  $n \times m$ , where  $n$  represents the number of zones or locations and  $m$  represents the total number of minutes in a day:

1. Location visit probability matrix ( $\mathcal{L}$ ) - Represents the probability of being at a specific location at any given minute of the day.



2. Location occupancy probability matrix ( $S$ ) - Represents the probability of remaining at a location for a specified duration.

The  $\mathcal{L}$  matrix is influenced by the time of day, while the  $S$  matrix depends on the location being visited. Fig. 7 illustrates how these matrices are utilized to model human motion. At any given moment, an individual is assigned probabilities for being at various locations. The higher the probability, the greater the likelihood of being at that location. The actual location a person visits is determined using the roulette wheel selection method applied to the matrix  $\mathcal{L}$ . Once a location is selected, the duration of stay at that location is determined using matrix  $S$  in a similar manner. After the stay duration ends, the process repeats with a new location and corresponding stay duration. This iterative approach is used to generate schedules for agents in the second stage of AVSim: ABM simulation.

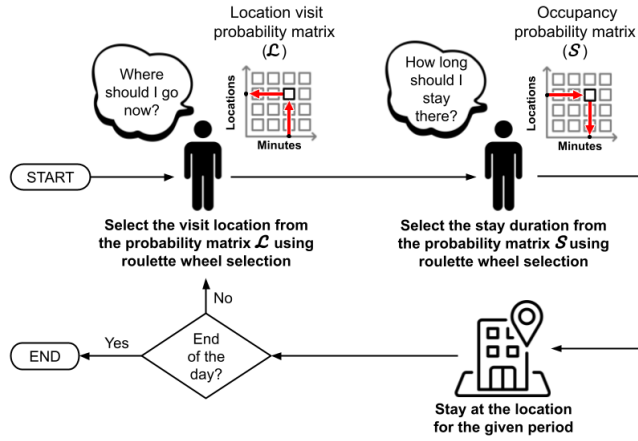


Figure 7: Process of generating daily trajectories.

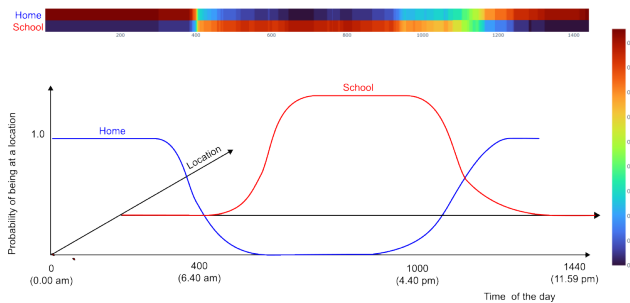


Figure 8: Probability variation for the most visited locations with time for Students.

Using the time-location dataset generated earlier, we extracted these two matrices for each profession class. Two rows extracted from a generated matrix  $\mathcal{L}$  are illustrated in Fig. 8. This figure shows the visit probabilities for two of the most visited locations for students throughout a regular school day.

## 2.2. Software system

AVSim was implemented using Python for its flexibility and extensive libraries for simulation and data processing. The class and object structure based on object-oriented principles were used to represent the system's agents, locations, and transport mediums. This approach improved code modularity, reusability, and ease of maintenance. For data visualization, a React application was employed, utilizing the React-D3-Tree library for visualizing tree structures. Python's Folium library was used to generate interactive maps.

## 2.3. Environment

To represent the geographical hierarchy identified in Section 2.1.2, we used a tree-based hierarchical structure to represent the environment within the ABM. This structure

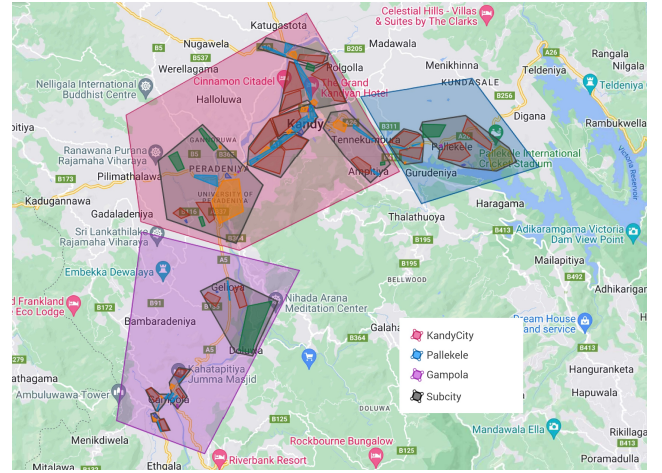


Figure 9: Map illustrating the Kandy District with annotated cities, sub-cities, and functional zones.

is advantageous as it allows agents to navigate between locations in a way that mirrors real-world movement. When an agent transitions from one location to another, the tree structure inherently defines the sequence of locations or zones it must traverse, which is essential for understanding and predicting the spread of disease.

Given that the motion data was sourced from the Kandy District in Sri Lanka, the same environment was recreated within the ABM framework. The district's geography, including its three major cities—Kandy, Pallekele, and Gampola—was annotated using polygon shapes on Google Maps. Each city was further subdivided into sub-cities and zones, classified based on their primary functions, such as educational, medical, and residential areas. For instance, schools located near each other within a city were grouped into a single educational zone. Fig. 9 illustrates the annotated cities and zones.

The annotations were exported, and the polygon coordinate points were used to construct the environment within the ABM. The hierarchical structure was built using the NetworkX library.

At the base level of the hierarchy, the tree's leaves represent primary locations such as schools, homes, and hospitals. These locations were randomly placed within designated zones (e.g., educational, residential, medical) to reduce manual annotation, as specific placements within zones have minimal impact on disease spread. The zones form the next hierarchical level. To differentiate locations and zones, a numbering system (e.g., "Home\_1," "Home\_2," "ResidentialZone\_1," "ResidentialZone\_2") was applied. These names were derived from the generated dataset to align with the created bimodal probability matrices.

Higher levels of the hierarchy represent broader geographical categories such as sub-cities, cities, and districts. ABM users can define areas based on their needs, regardless of the generated dataset. Fig. 10 illustrates the tree structure, with only a single zone expanded to show its locations for clarity.

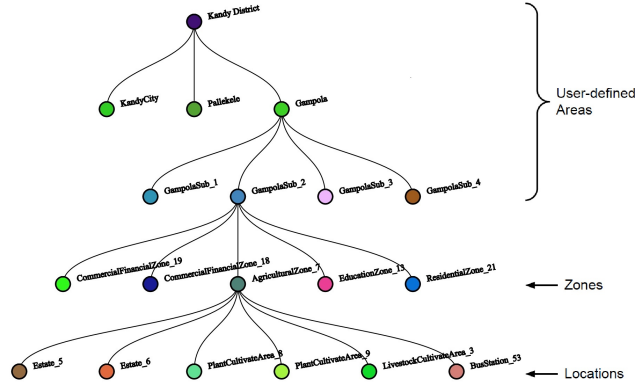


Figure 10: Hierarchical tree structure of the environment.

In this tree structure, each node represents a geographical area. Nodes are implemented as objects, with attributes defining each area's characteristics, including its boundary (polygon coordinates), centroid, and the list of agents present. Each node also contains a dictionary to track the number of agents and their respective disease states.

## 2.4. Vector patch

In agent-based models of vector-borne diseases, it is not essential to represent each vector individually, as is done for human agents. Instead, modeling vector density within localized areas provides a simpler yet accurate representation of the vector population. Following approaches from similar studies [14], the simulation adapts a patch-based approach to represent vector densities.

Each zone is divided into patches, with the patch size determined by the approximate habitat areas of the vectors. Fig. 11 presents a map of Kandy City, illustrating an example of vector density across different patches.

A patch is modeled as an object that encapsulates environmental factors such as temperature, humidity, and rainfall, which influence vector emergence and death rates. It also maintains the number of vectors in different disease

states, a dictionary of agents with their disease statuses, and a list of locations within the patch.

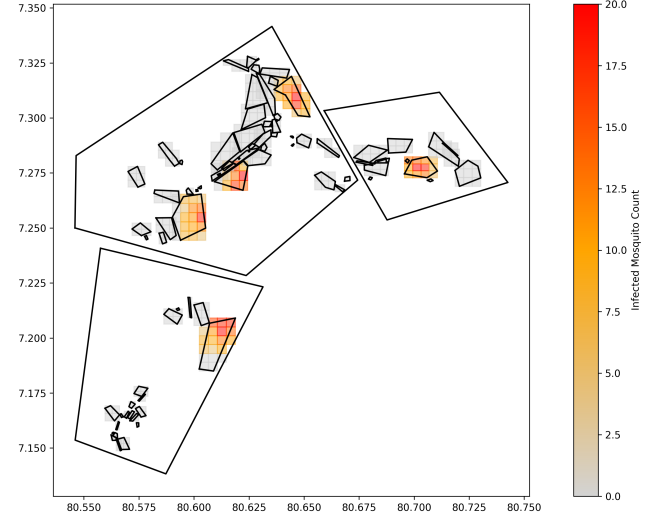


Figure 11: Map of Kandy District showing the zones and their patches, with a color bar representing an example vector density across the patches

The total birth rate of vectors in a given patch  $k$ ,  $h_v^k$ , is calculated as follows:

$$h_v^k = N_v^k \left( \psi_v - (\psi_v - \mu_v) \cdot \frac{N_v^k}{K_v} \right) \quad (6)$$

where:

- $\psi_v$ : Average natural emergence rate of vectors
- $\mu_v$ : Average death rate of vectors
- $K_v$ : Carrying capacity of the vectors in the patch
- $N_v$ : Total number of vectors in the patch

## 2.5. Agent generation and emulation

The agents of the system are a vital component in any agent-based model. In this model, agents were initially categorized based on their occupation class and further subdivided as per the identified mobility patterns. For instance, doctors who worked the day shift vs. the night shift were classified into two groups. Each occupation class was defined as either an adult or child class. This parameter was important to establish the independence of each occupation class. The occupation classes, sub-classes and composition of agents to be modeled by the ABM could be varied based on input data.

The agents were represented through the use of Object Oriented Programming (OOP) concepts, specifically classes and objects. The agent class represented the structure of all agents (objects) created for emulation. Parameters of an agent defined the characteristics of each individual agent, such as the occupation class, sub-class (if applicable), age



ranges, home and work location classes, and factors necessary for disease modeling. The total count of agents was dependent on the carrying capacity of the environment. As mentioned in the above sections, this study was capable of modeling the Kandy district, and approximately 2000 agents were generated for emulation. This constituted about 1% of the actual population of the district. The composition of agent occupation classes was also selected to approximately represent their real-life counterparts.

The procedure of agent generation within the ABM was as follows. At the start of emulation, the ABM was given the carrying capacity and composition of agents from the environment and input data, respectively. The agent objects were then generated with parameters set within defined ranges for the respective occupational classes. Subsequently, each agent object was assigned a home object. The occupancy limit for home objects is defined by the emulation parameters. Each house object was constrained to either be empty or to contain one or more adult agents. This was due to child agents not being considered independent in the ABM. Finally, a work location object corresponding to the agent's work location class was assigned to the agent at random.

Upon completion of the agent generation procedure, the emulation process was initiated. Simulation steps were executed every 1 minute for each day (resolution of the simulation). At the start of an emulation day, a timetable was generated for each individual agent (this process is described in Section 2.1.4). This timetable defined the routine (in terms of locations to visit and time of occurrence) for each agent. Except for home and work locations, all other locations (such as shopping malls and banks) were given as location classes. Therefore, the agent would choose to visit the closest location instance of that class. Once the timetables were generated, each agent would utilize modes of transport (as explained in the next section) to follow their schedule.

## 2.6. Transport

In the context of disease modeling, long-range human mobility plays a critical role in facilitating the rapid geographical dissemination of emergent infectious diseases [36]. This study incorporates the simulation of long-range human mobility by modeling both private and public transportation systems to better understand their impact on disease spread.

In the private transport modeling approach, a subset of agents was designated with a public transport medium flag, while others were assigned private transport objects at the simulation's outset. These private transport objects enabled agents to travel to their destinations whenever needed. Conversely, agents marked with the public transport medium flag utilized public transport for all instances of long-range mobility. The primary objective was to evaluate the impact of private transport users on disease propagation.

Public transport modeling holds significant importance in the context of disease modeling, particularly due to the increased vulnerability of passengers to airborne disease

transmission in confined spaces with close proximity to others [37]. Agents not assigned a private transport medium flag relied on public transport for long-range mobility instances.

In this study, buses and taxis were used as the primary modes of public transport. Two types of bus objects were employed to represent different hierarchical levels in the simulated environment. Inter-city buses facilitate transport between cities, while intra-city buses facilitate transport inside a city. This process is explained in Fig 12.

Bus objects were initiated at the start of the simulation. Each bus station referred to as a Bus Node, maintained an updated dictionary of available buses and their next destinations. When a bus arrived, agents who had been waiting

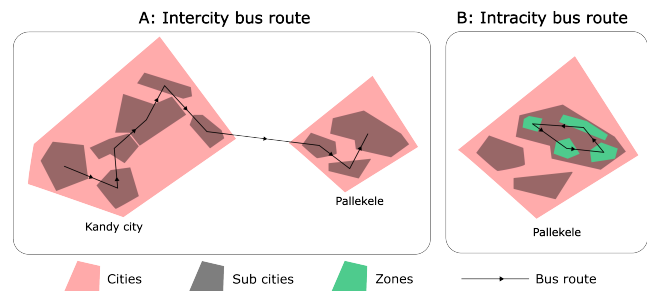


Figure 12: Public transport mechanism.

for transportation were assigned to that bus, provided the bus's next destination matched the agent's next location in the bus's dictionary of destinations.

If the agent had to wait too long for a bus, they would be assigned to a taxi to travel to the next destination. The Taxi was assigned to each zone so that every agent who missed the bus could still get a taxi. When a taxi arrived at a destination zone, it stayed there until the next trip was assigned.

## 2.7. Markov disease progression model

A person can transition through various states after being exposed to a disease. These transitions depend on the nature of the disease. Generally, an exposed individual becomes infectious after a certain period, carrying the risk of spreading the disease. The disease progression may remain asymptomatic or exhibit symptoms, potentially progressing through severity stages such as mild, severe, and critical.

We used a Markov model to handle state transitions, as illustrated in Fig. 13, which defines the possible states a person can be in after exposure to a virus. Transitions between these states were probabilistic and were often modeled using distributions such as the log-normal distribution. The probabilities of these transitions depended on factors like the nature of the disease, age, prior infections, and the quality of medical care. For our two use cases, dengue and COVID-19, the transition times are shown in the figure and followed a log-normal distribution. Values for COVID-19 were taken from Covasim [7] while dengue was taken from WHO [38].

It is important to note that the transition from the "susceptible" to "exposed" state was not considered part of the Markov model. This transition depends on how a person

becomes exposed to the virus. In airborne diseases, this typically occurs through human-to-human contact, while in vector-borne diseases, it happens via interactions with vectors. These mechanisms will be detailed in subsequent sections.

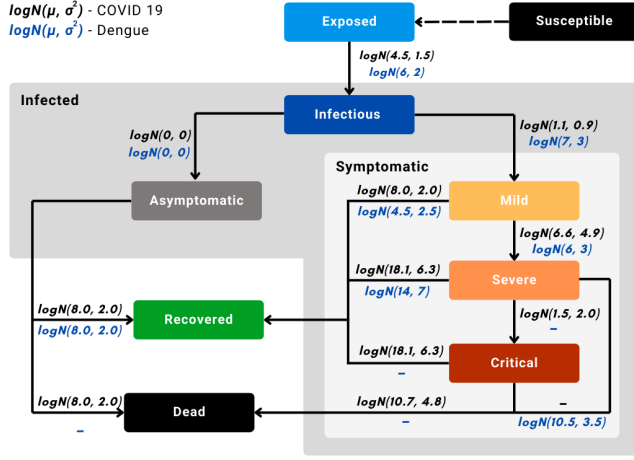


Figure 13: Markov model for disease transmission modeling.

In this model, we had  $N$  possible states (without "susceptible"), and transitions between these states were represented by the transition matrix  $A$ , where  $A_{ij}$  denotes the probability of transitioning from state  $j$  to state  $i$ . We used a probability vector  $p_t$  (of size  $N \times 1$ ) that captures the state probabilities at time  $t$ . To find the next state probabilities  $p_{t+1}$ , we applied the fundamental equation 7 for a Markov chain.

$$p_{t+1} = A \cdot p_t \quad (7)$$

To determine the actual next state, we generated a random number  $r$  between 0 and 1. Using  $p_{t+1}$ , we calculated cumulative probability ranges for each state  $i$ , based on the probabilities in  $p_{t+1}$ . The next state is chosen as the one for which  $r$  falls within the cumulative range associated with that state.

## 2.8. Air borne disease modeling

### 2.8.1. Disease progression mechanism

Initially, a small percentage of the population was infected with the COVID-19 virus, and the agents were freely allowed to go about their daily business, allowing us to study the disease spread. Once an agent is infected, it will progress through different stages of the disease. This was modeled using the Markov model as shown in Fig 13. Each agent will belong to either susceptible, exposed, infectious, symptomatic, asymptomatic, or dead states.

The disease is spread when a susceptible individual comes into contact with an infected one. Contacts occurred in two scenarios: at specific locations or during transport (on a bus). At each time step, a 1-meter radius around each agent was monitored. If another agent enters this radius, it is recorded as a contact. When a susceptible agent contacts an

Table 2

Age-based susceptibility values for agents

Age	0-9	10-19	20-69	70-79	80+
Susceptibility	0.34	0.67	1.00	1.24	1.47

infected agent, a random number is generated. If this number recedes the agent's infectious probability ( $\rho$ ), the susceptible agent's disease state changes to "exposed." Each agent's disease state is then updated according to the disease model. Agent's infectious probability depends on the individual's immunity level, as described in the following section.

### 2.8.2. Immunity modeling

Contact between a susceptible agent and an infected agent does not always result in disease transmission. This is determined by a transmission probability, which depends on the agent's immunity. In the simulation, agents were assigned varying immunity levels based on factors such as age, hygiene practices (e.g., maintaining a safe distance, hand washing, sanitizer use), and vaccination status. This infection probability,  $\rho$ , can be modeled using the equation 8.

$$\rho = S_{age} \cdot k \cdot (1 - \alpha_{vacc}\gamma_{vacc} - \alpha_{hyg}\gamma_{hyg}) \quad (8)$$

where  $S_{age}$  is the susceptibility based on the age,  $k$  is a tunable parameter that has to be manually found,  $\alpha_{vacc}$  is the Weight assigned to vaccination,  $\gamma_{vacc}$  is the Immunity boost provided by vaccination,  $\alpha_{hyg}$  is the Weight assigned to hygiene factor and  $\gamma_{hyg}$  is the Immunity boost provided by safe hygiene practices which include washing hands, wearing masks, and social distancing. The age-based susceptibility values were taken from Covasim [7], and they are presented in Table 2. Through some prior tuning process, the value of  $k$  was selected as 0.3.

### 2.8.3. PCR testing and quarantine mechanism

Polymerase Chain Reaction (PCR) testing is crucial in predicting the risk of airborne diseases [39]. This is used as a pre-event testing activity, and people with positive PCR results are identified as infected agents. In the COVID-19 pandemic, infected agents were identified using PCR tests and using contact tracing methods. Contacted agents were subjected to quarantine or self-isolation [40].

The AVSim had the functionality to perform PCR tests to identify the infected agents. Each agent would have a daily testing probability, which would depend on the state of infection. This method allowed the user to specify the testing probabilities for each of these states. These numbers would depend on the regulations of the government and the healthcare sector. Therefore, the simulation would decide the number of PCR tests done each day.

Two methods were employed in the simulation to perform quarantine. In the first method, if a PCR test was positive, the relevant agent would be isolated and put under quarantine. When that agent was recovered and safe to interact with other agents, the simulation would allow the agent to

**Table 3**

Different types of possible vaccines and their effectiveness

Vaccine Name	Immunity boost after 1st dose	Immunity boost after 2nd dose
Moderna	74	93
AstraZeneca	78	67
Pfizer	84	93

end their quarantine. In the second method, all agents within a specific occupation class were quarantined if the number of infected agents in that class surpassed a certain threshold. In 3.3, results for each of these methods are analyzed and discussed.

#### 2.8.4. Vaccination mechanism

Vaccination mechanisms are utilized to enhance community immunity, particularly during outbreaks of airborne diseases like COVID-19 [41]. In AVSim, vaccination events were organized to reduce the disease spread while increasing the immunity levels of the agents.

In AVSim, an outbreak was declared whenever the total number of infected agents exceeded a specified threshold. When an outbreak was detected in the simulation, vaccination events could be organized. The AVSim simulation allowed the organization of vaccination events on a selected day at a specified geographical zone. AVSim further allowed the capability to vaccinate targeted occupational classes and gave out various types of vaccines. When an agent is given a vaccination, their vaccine immunity  $\gamma_{vacc}$  is boosted. According to [42], a few possible vaccine types and their immunity boosts are shown in Table 3. New vaccination events with new vaccine types could be added this way. Additionally, vaccination could be administered in doses.

### 2.9. Vector-borne disease modeling

For modeling vector-borne diseases, the network-patch approach proposed by Carrie Manorea et al. [14] for dengue transmission has been adapted in this study to reflect the dynamics of vector-borne diseases more accurately.

#### 2.9.1. Disease progression in vectors

As mentioned in Section 2.4, we do not consider individual vectors separately. Instead, we used a patch to represent vector density and employed a stochastic process to model disease progression. Specifically, we focused on three disease states of the vectors: susceptible, exposed, and infected, as illustrated in Fig. 14.

Each patch  $k$  is initialized with counts for susceptible ( $S_v^k$ ), exposed ( $E_v^k$ ), and infected ( $I_v^k$ ) vectors, ensuring that these values remain below a defined vector carrying capacity specific to each patch. The temporal dynamics of vector density within a patch are modeled using a system of differential equations. The changes in vector counts for a given patch  $k$  are determined as follows. Factors with superscript  $k$  are unique to a given patch, while others are patch-independent.

$$\frac{dS_v^k}{dt} = h_v^k - \lambda_v^k S_v^k - \mu_v S_v^k \quad (9)$$

$$\frac{dE_v^k}{dt} = \lambda_v^k S_v^k - v_v^k E_v^k - \mu_v E_v^k \quad (10)$$

$$\frac{dI_v^k}{dt} = v_v^k E_v^k - \mu_v I_v^k \quad (11)$$

where:

- $h_v^k$ : Total birth rate of vectors
- $\lambda_v^k$ : Average infection rate of vectors
- $v_v^k$ : Average rate of progression of vectors from exposed state to infectious state
- $\mu_v$ : Average death rate of vectors


**Figure 14:** Mosquito state transition.

The average infection rate of vectors in patch  $k$ ,  $\lambda_v^k$ , is calculated as follows:

$$\lambda_v^k = b_v^k \cdot \beta_{vh} \cdot \left( \frac{I_h^k}{N_h^k} \right) \quad (12)$$

where:

- $b_v^k$ : The number of bites per vector per unit time
- $\beta_{vh}$ : The probability of transmission from an infectious agent to a susceptible vector given that contact between the two occurs
- $I_h^k$ : The number of infected agents in the patch  $k$
- $N_h^k$ : Total number of agents in patch  $k$

The number of bites per vector per unit of time in patch  $k$  which is defined in the following way:

$$b_v^k = \frac{b^k}{N_v^k} \quad (13)$$

where:

- $b^k$ : The total number of contacts between agents and vectors (bites) in patch  $k$  per unit time

**Table 4**  
Parameters for dengue simulation

Parameter	Value/Range
$\psi_v$ : Average natural emergence rate of mosquitoes	0.3
$\mu_v$ : Average death rate of vectors	1/14
$\sigma_v$ : The maximum number of bites per vector per day	0.5
$\sigma_h$ : The number of bites a human can get per day	10
$K_v$ : Mosquito carrying capacity	[100-200]
$\beta_{vh}$ : The probability of transmission from an infectious agent to a susceptible mosquito	0.33
$\beta_{hv}$ : The probability of transmission from an infectious mosquito to a susceptible agent	0.33

The total number of contacts between agents and vectors (bites) in patch  $k$  is defined in the following way:

$$b^k = \frac{\sigma_v \cdot N_v^k \cdot \sigma_h \cdot N_h^k}{\sigma_v \cdot N_v^k + \sigma_h \cdot N_h^k} \quad (14)$$

where:

- $\sigma_v$ : The maximum number of bites per vector per unit time.
- $\sigma_h$ : The number of bites a human can get per unit of time.

For the selected use case of dengue virus infection, the average rate per agent of progression from the exposed state to the infectious state of vectors in patch  $k$ , denoted as  $v_v^k$ , depends on the temperature [43] and was calculated as follows:

$$v_v^k = \frac{1}{tinc_v^k} \quad (15)$$

where:

- $tinc_v^k$ : The incubation time of the virus in the mosquito in patch  $k$ . This depends on the temperature of the patch ( $T^k$ ) and is calculated as follows:
  - If  $T^k < 21$ , then  $tinc_v^k \sim U(10, 25)$
  - If  $21 \leq T^k < 26$ , then  $tinc_v^k \sim U(7, 10)$
  - If  $26 \leq T^k < 31$ , then  $tinc_v^k \sim U(4, 7)$

The parameters used for dengue transmission [38] are provided in Table. 4, with rate values specified on a per-day basis. Since the model includes multiple vector patches, a range of values was selected for some parameters, indicating minimum and maximum values (enclosed in brackets).

## 2.9.2. Disease progression in agents

The infection rate of agents from infectious mosquitoes is determined by the frequency of bites an agent receives, the likelihood that the bite is from an infectious mosquito, and the probability that the infection will be successful given the bite. This rate can be represented as:

$$\lambda_{k,h}(t) = b_h^k \cdot \beta_{hv} \left( \frac{I_k^v}{N_k^v} \right) \quad (16)$$

where:

- $b_{k,h}$ : the number of bites an agent receives per unit time from mosquitoes in patch  $k$
- $\beta_h$ : the probability of successful infection given a bite from an infectious mosquito
- $I_k^v$ : the number of infectious mosquitoes in patch  $k$
- $N_k^v$ : the total number of mosquitoes in patch  $k$

To calculate the probability of a susceptible agent becoming infected, the infection rate must be converted into a probability of infection within a given time step. We run the simulation and update agent movements in time steps of  $\Delta t$ , while the disease states of agents and vectors are updated every  $n \cdot \Delta t$  time steps. In our simulation, agent movements are updated every 1 minute, and disease statuses are updated every 5 minutes. Assuming the time to infection follows an exponential distribution [14], the probability of infection at the end of the time interval  $\Delta t$  is given by:

$$p_k = 1 - e^{-\lambda_{k,h}\Delta t} \quad (17)$$

where:

- $p_k$ : infection probability of a susceptible person in patch  $k$
- $\lambda_{k,h}(t)$ : infection rate of an agent

Then, a random variable between 0 and 1 is generated every 5 minutes to check if it falls above the infection probability. If the random variable exceeds the probability, the agent is marked as exposed. Once an agent is exposed, the disease transitions follow the Markov model as shown in Fig. 13.

An infected person may either stay asymptomatic, develop mild symptoms, or, in rare cases, progress to severe symptoms [38]. Many people with dengue remain asymptomatic, showing no visible symptoms. Those with mild symptoms experience typical dengue signs like fever, headache, and body aches, which often resolve with basic supportive care, allowing for full recovery. Severe dengue, however, can bring serious symptoms like intense abdominal pain, persistent vomiting, bleeding, or shock, often requiring hospitalization and posing life-threatening risks.



The likelihood of transitioning between these states depends on various factors, including age, prior dengue infections, and the quality of medical care. For instance, the likelihood of an infected person developing symptoms may vary based on their immune response.

The Markov model outlined in Section 2.7 is used to determine state transitions. For dengue, the model focuses only on mild and severe symptomatic states. By combining probabilistic state transitions with random transition periods, the model can effectively simulate diverse disease progression outcomes among individuals.

### 2.9.3. Hospitalization mechanism

There is a high probability of symptomatic patients visiting the hospital. At the start of each day in the simulation, all agents' disease statuses are checked. If symptomatic agents are present, a random hospitalization probability is generated. If this probability exceeds a certain threshold, the agent is hospitalized. For severe cases, this threshold is lower, reflecting the higher likelihood of hospitalization. In our simulation, we used 0.4 for mild cases and 0.9 for severe cases.

Once the agents requiring hospitalization are identified, they are removed from both the environment and the patches and placed in a virtual space. Hospitalized agents do not contribute to further disease spread. However, their disease states continue to update as outlined in Fig. 13. Eventually, these agents either recover or die. Recovered hospitalized agents are returned to both the environment and their respective patches.

### 2.9.4. Intervention mechanism

When there is a rise in reported vector-borne cases in a specific area, vector control interventions are initiated, often spearheaded by government healthcare programs or community efforts. These measures typically include mosquito spraying or the removal of breeding sites.

In AVSim, to simulate such interventions, the total mosquito-to-host exposure in each patch is recorded. If the cumulative number of exposed agents in a zone over one week surpasses a predefined threshold,  $E_h^k$ , the vector population in the affected zone's patches is reduced by  $m\%$  to represent mosquito spraying and the elimination of breeding sites.

## 3. Results and discussion

### 3.1. Spectral clustering results

Distinct behavioral patterns within each occupation class were derived by applying the Spectral Clustering algorithm to each occupation class. This was done by manual inspection of the output of the clustering algorithm. Table 5 presents the synthesized results. Note that normal behavior refers to a typical workday for each class.

After examining the results, it can be observed that the algorithm excels at producing clusters with distinct behavioral patterns, ranging from regular work routines to holiday behaviors in alignment with real-world intuition.

**Table 5**

Distinct behavioral patterns Obtained for occupation classes through spectral clustering method.

Class	Identified Clusters
Animal Farmer	Work area is located in close proximity to the residence.
	Work area is situated separately from the residence.
	Individual resides and works within a designated Agricultural Zone.
Bank Worker	Normal workday behaviour
	Weekend and holiday behaviour
Doctor	Normal workday behaviour
	Night to evening shift
	Night to morning shift
	Weekend and holiday behaviour
	Night shift at the hospital with daytime duties at a school medical center
Farmer	Work area is located in close proximity to the residence.
	Work is conducted within an Agricultural Zone.
Garment Admin	Weekend and holiday behaviour
	Normal workday behaviour
Garment Worker	Work area is located separately from the residence.
	The individual resides in or close to the work area.
Sales Rep	Normal workday behaviour
	Holiday behaviour
Student	Normal behaviour of a student travelling from home
	Weekend and holiday behaviour with irregular school attendance
	Hostel student
Super Market Worker	Morning to night shift behaviour
	Afternoon to night shift behaviour
	Morning to evening shift behaviour
	Works from morning to afternoon & evening to night with a break in between. also includes holiday behavior
Teacher	Teacher resides in or near the school premises
	Normal teacher behaviour (travelling from home)
	Weekend and holiday behaviour

Furthermore, the algorithm effectively filters out anomalous patterns, as demonstrated in the instances above. The final results and the human motion dataset we created to fuel the AVSim can be found online at [44].



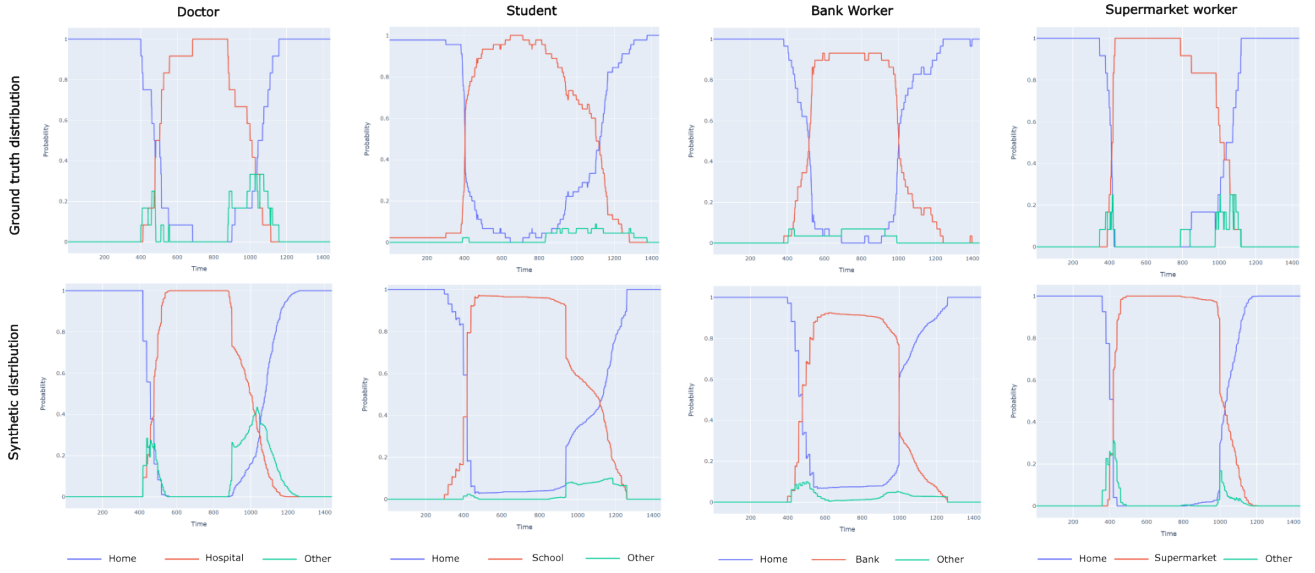


Figure 15: Validation of bimodality.

### 3.2. Validation of human motion modeling

To validate the accuracy of the human motion model, 10000 samples of daily person trajectories were generated for each profession class. Then, the probability distributions were reconstructed using them to compare with the original probability distributions. These synthetic and original plots can be seen in Fig. 15. We can see that the synthetic distributions closely resemble the ground truth distributions, thus proving the above method to be highly accurate in replicating human behavior.

### 3.3. Air borne disease simulation results

In this sector, a few simulations were conducted to research air-borne disease spread. However, it is important to note that these results are only aligned through a subset of possible research directions. One can perform various analyses based on their need and interests. The simulations were conducted in a simulated environment replicating the Kandy district.

#### 3.3.1. Contact tracing

By default, the AVSim will generate detailed descriptions of each agent in the simulation, such as daily routines, daily person trajectories, disease progression history, and daily contacts. This is illustrated in Fig. 16. The AVSim can be customized to generate any other required information.

The ability to trace back contacts is a key feature that is crucial in any type of ABM. Fig. 17 shows the locations where the disease was transmitted from an infected agent to a healthy agent. This is essentially the contact tracing mechanism of the ABM in action. When analyzing, it can be seen more contacts are present in the "Residential Zones." This can be described as the area of houses compared to other places being lower. Therefore, there is a high possibility of more contact in houses. Also, another major observation is that although there are higher contacts in residential zones,

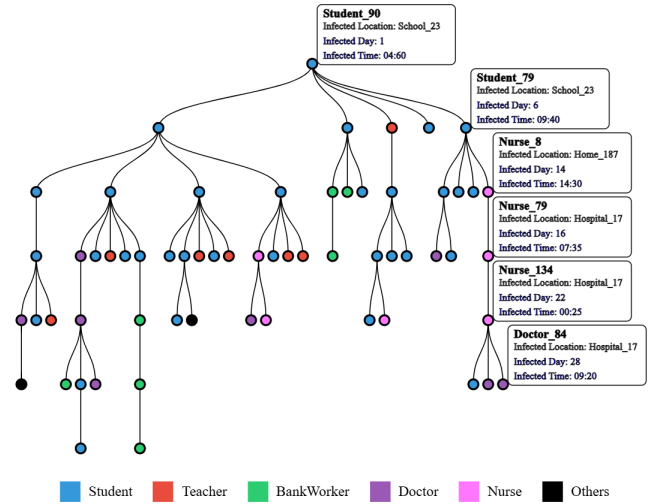
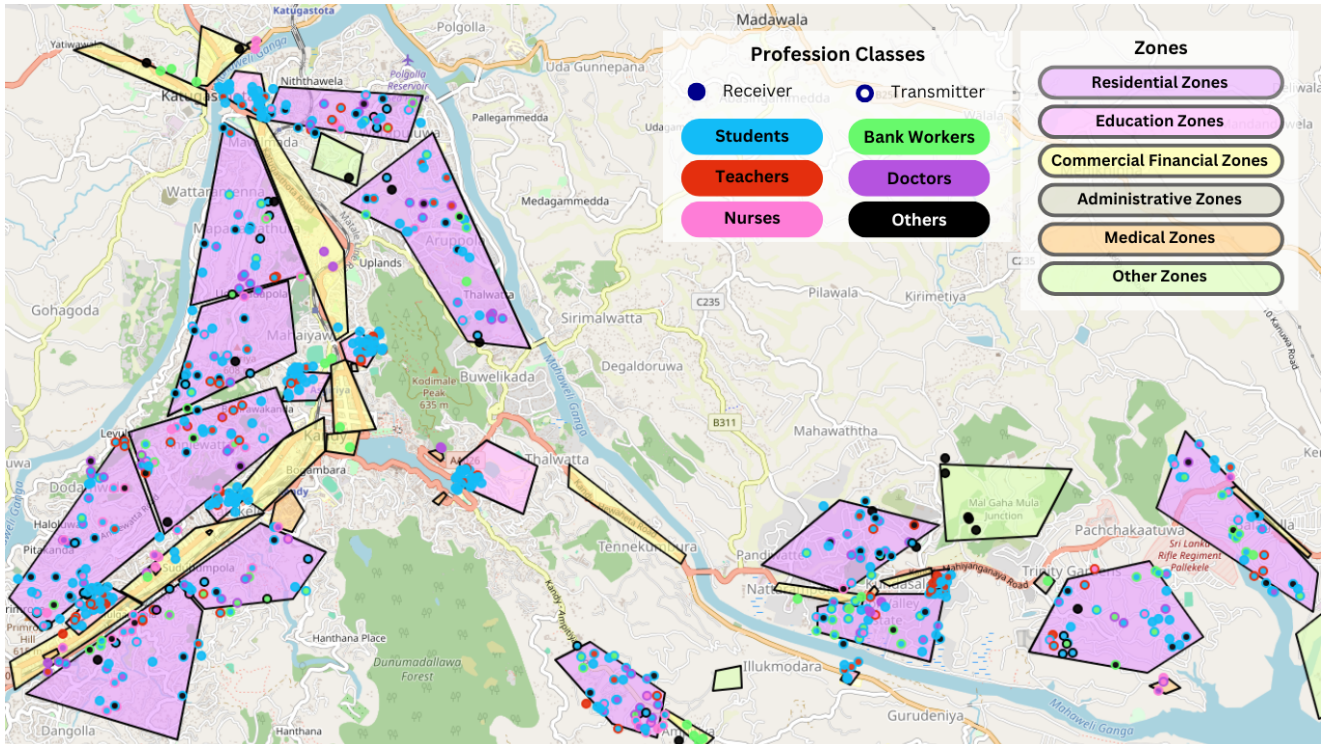
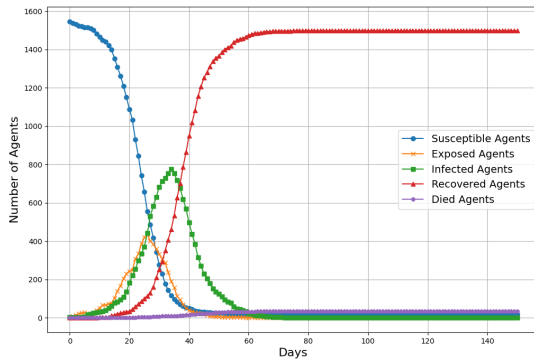


Figure 16: Contact tracing capability of AVSim.

the spread of disease to other communities, i.e., residences present in other cities, is by contacts in work locations or outside. This can be verified by Fig. 16. Starting with one infected student agent, the disease transmits to another student agent at the school. Then, the received student agent transmits the disease to the nurse at the student agent's home. This leads to the spread of disease in a hospital, which is the working location of the nurse. Likewise, it can be observed that there are several branches of contact between the second student who was contacted and the initial student at the school. It proves work locations (here, a school for the student and a hospital for the nurse) are involved in spreading diseases to different communities through the agents in the same work locations. Therefore, identifying these kinds of contact patterns and predictions at early stages will enable policymakers to pinpoint high-risk areas and implement



**Figure 17:** All the contacts in an uncontrolled, i.e., no vaccine nor quarantine disease-transmitting moment for 50 days simulation in a part of "KandyCity" and "Pallekele." Initially, three students were infected randomly. The receiving agent is shown by filled circles and the cause; the transmitting agent is shown by outer borders in each instance.



**Figure 18:** Agents count in different states in an uncontrolled epidemic outbreak, which started with three infected students.

targeted interventions to prevent the spread of the disease in these regions.

### 3.3.2. Disease progression in an uncontrolled environment

This AVSim simulation can be executed without imposing policies to reduce the spread, which is known as an uncontrolled environment. Fig. 18 shows an uncontrolled epidemic outbreak where three random student agents were initially infected. We can see that this plot closely resembles

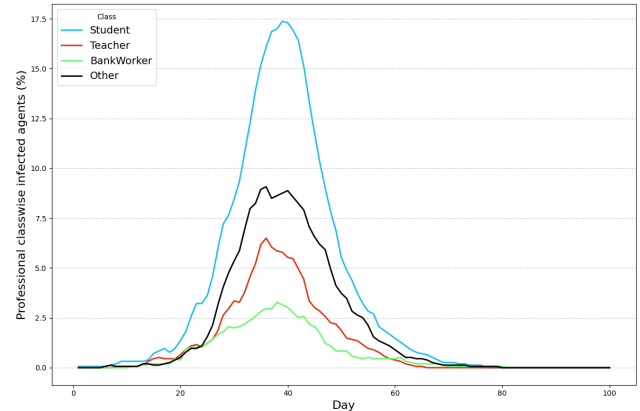


**Figure 19:** Disease spread in different professional classes in an uncontrolled epidemic outbreak which started with three infected students.

the theoretical SEIR model curve, hence validating the practical approach of AVSim.

### 3.3.3. Effect of initially infected agents on disease progression

The AVSim allows the analysis of disease spread patterns when agents from a specific class were initially infected. To demonstrate this, three students were initially infected in an uncontrolled environment, and then the disease

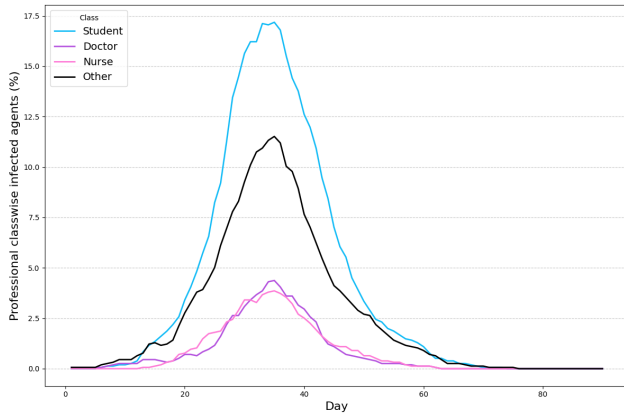


**Figure 20:** Disease spread in different professional classes in an uncontrolled epidemic outbreak which started with three random infected agents.

spread to other classes over the simulation days was observed. The Observations are shown in Fig.19, highlighting only the top three classes that had the highest percentage of infected agents. For approximately up to 50 days, a considerable percentage of the disease was spread to teachers, w.r.t. other classes. This is reasonable because contact from students is mostly present in schools, which is the work location of teachers. This analysis helps identify the most vulnerable groups to the disease concerning initial infection.

Furthermore, it can be observed that the spread to other classes in Fig. 19 becomes higher when the days pass, showing the effect of contacts in an uncontrolled environment. When the agents are randomly infected, it is hard to predict a pattern of spreading to other classes, and it depends on contact tracing. For example, in the simulation provided by Fig 20, when the agents were randomly selected, initially infected agents were one student, one doctor, and one teacher. However, in that case, disease spread had a significant impact on the medical sector agents. One key observation from the two simulations mentioned above is that the student class is consistently more affected. This is because most agents in different professional classes have student agents in their residences, where they will interact more with student agents. Therefore, more controlled strategies should be implemented to minimize the risk of disease spread to other classes from these vulnerable groups.

### 3.3.4. Quarantine and vaccination measures

We have tested several controlled mechanisms to reduce the spread of airborne diseases. The following conclusions were assumed based on the parameters that we set as described in the 2.8 section.

A Effect of Quarantine: Fig. 21 shows the number of infected agents in different quarantine mechanisms compared to uncontrolled cases. The AVSim allows two mechanisms in quarantine: quarantine by profession class and self-quarantine of individuals when PCR results are positive. It can be observed that when

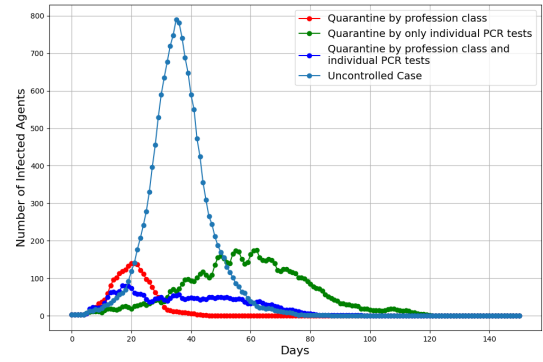


**Figure 21:** Effect of quarantine mechanism in airborne diseases w.r.t. uncontrolled case.

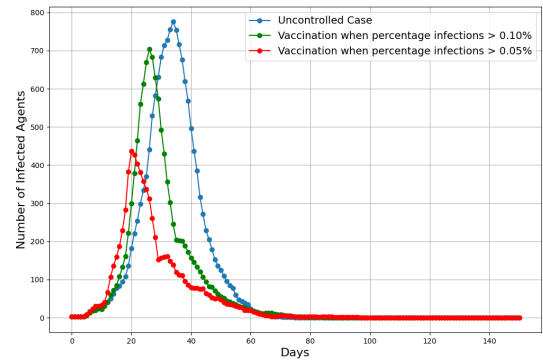


**Figure 22:** Effect of vaccine mechanism in airborne diseases w.r.t. uncontrolled case.

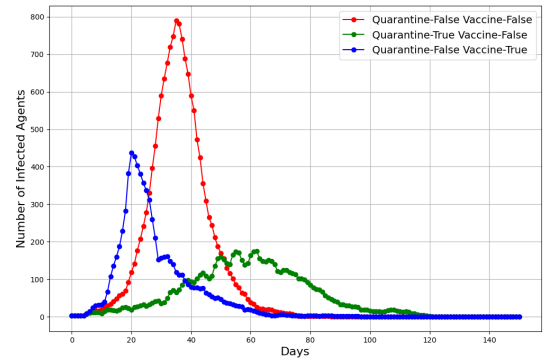


**Figure 23:** Effect of quarantine and vaccination mechanism in airborne diseases.

combined mechanisms are used, the peak of infected agents is reduced by approximately 87.5%.

B Effect of Vaccine: Fig. 22 shows the number of infected agents in different vaccine mechanisms compared to uncontrolled cases. We analyzed the effect of

vaccinating all the agents when the infected percentage of the population is greater than 5% and 10%. It can be deduced that early vaccination events cause a higher disease spread reduction.

- C Controlled vs. Uncontrolled cases: Fig. 23 shows the number of infected agents in controlled via vaccination or quarantine and uncontrolled cases. It can be observed that a higher reduction in disease spread was obtained from proper quarantine mechanisms.

### 3.4. Vector-borne disease simulation results

The simulations were conducted with 2000 individual agents, using Kandy District as the simulation environment. The transportation model was not included in the simulation, based on the assumption that vector bites do not occur in public transportation.

The *Aedes aegypti* mosquito typically flies up to 400 meters in search of water-filled containers to lay eggs, but it generally stays near human habitation [38]. Our simulation used a 500x500 square meter patch size to represent the mosquito's activity area. The other simulation parameters or ranges are specified in Table. 4.

#### 3.4.1. Disease progression in an uncontrolled environment

At the beginning of the simulation, the patches and locations were initialized with agent and vector counts. Six homes were chosen from a designated residential zone, with up to five agents per home initially marked as exposed to dengue. The nearest nine patches around each home were given an infected vector count ranging from 0 to 20. During the simulation, the patches were updated daily, and the disease propagated accordingly.

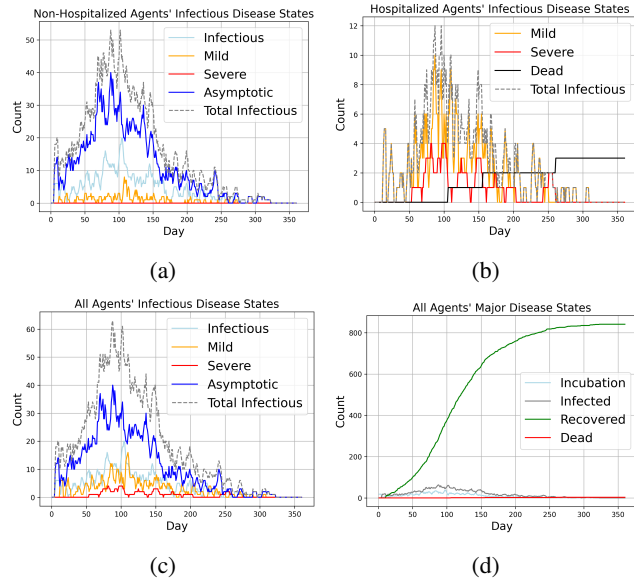
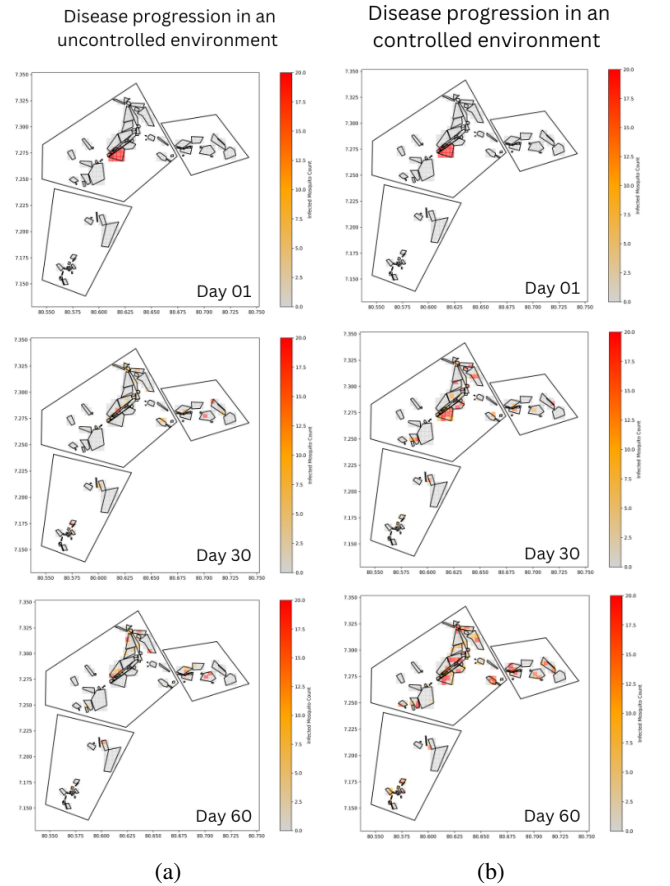


**Figure 24:** (a) Infectious disease states of non-hospitalized agents, (b) infectious disease states of hospitalized agents, (c) infectious disease states of all agents, and (d) major states changes of all agents over time.

At the start of the simulation, changes in the disease state of agents can be observed over time, as shown in Fig. 24. Analyzing the rate of change indicates that once dengue starts spreading, the infection rate gradually increases before eventually declining. However, in this simulation, each individual can only be infected once. If reinfection were allowed, the infection rates would likely be higher. Reinfection could be modeled by resetting recovered agents to a susceptible state, but for simplicity, this is not considered in this simulation.

#### 3.4.2. Disease progression in a controlled environment

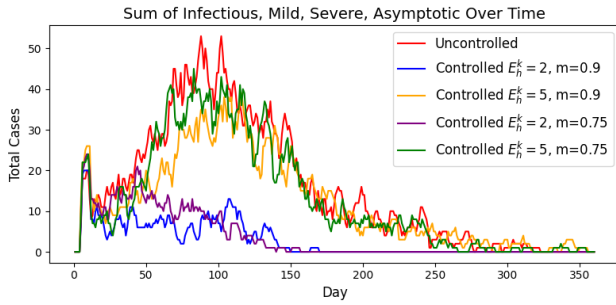
Various strategies can be employed to control dengue. In this simulation, the focus is on managing mosquito populations. If the cumulative number of exposed agents in a zone over an  $n$ -day period exceeds a predefined threshold,  $E_h^k$ , the vector population in the affected zone's patches is reduced by  $m\%$ . This reduction represents interventions such as mosquito spraying and the elimination of breeding sites. Fig. 25 illustrates a case where  $n = 7$ ,  $E_h^k = 2$ , and  $m = 75$ .



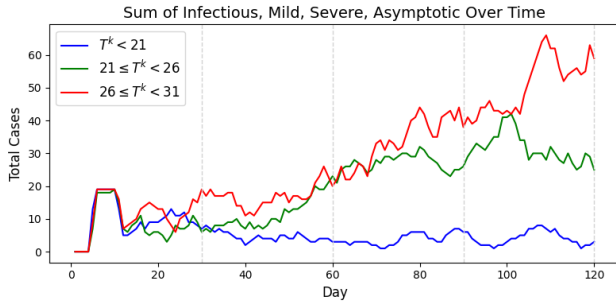
**Figure 25:** The infected vector count changes over 2 months in (a) an uncontrolled and (b) controlled environment.

Fig. 26 illustrates the mosquito control strategy under different scenarios. As the infection count increases, the number of exposed individuals in each zone also rises. At the end of each week, zones with more than  $n$  exposed agents undergo vector reduction. However, when higher thresholds for exposed counts are allowed, it becomes evident that this





**Figure 26:** The effect of controlling mosquitoes



**Figure 27:** Effect of temperature on dengue disease progression

strategy is not significantly different from the uncontrolled case.

In contrast, when control measures are implemented even for a small number of recorded cases, the strategy proves more effective. However, this comes with an economic trade-off. By using AVSim, it is possible to determine the optimal threshold for recorded cases to trigger control measures and the extent of control needed.

In the given example, while 90% control is the most effective, applying 75% control can also significantly reduce mosquito populations and, consequently, dengue cases.

### 3.4.3. Effect of temperature

As mentioned in Section 2.9.1, the average rate of progression of vectors from the exposed state to the infectious state depends on the mosquito's incubation time. The mosquito incubation time is highly influenced by temperature. Fig. 27 shows how the total infectious agent count changes as the mosquito incubation period varies with temperature. During high-temperature seasons, it is important to implement necessary measures to reduce the propagation of dengue.

## Funding

This research was funded by the International Development Research Centre, Canada, grant number 109586-001.

## Declaration of competing interest

The authors declare that they have no known competing financial interests or personal relationships that could have appeared to influence the work reported in this paper.

## 4. Conclusion

The emerging threat of air-borne and vector-borne diseases has existed forever in human history. Recent events such as the COVID-19 pandemic and the continuous spread of dengue fever are key examples of this. Some countries have faced severe consequences since they were not able to manage the spread of the disease by executing effective policies. In our study, we present AVSim, an agent-based model designed to assist policymakers in making more informed decisions for the effective control of diseases by taking in to account numerous possible scenarios.

AVSim sets itself apart by its ability to model complex real-world environments, a feature many other agent-based models lack. It can precisely simulate entire cities, subdivisions, zones, and even individual households. By leveraging demographic data of the modeled geographical area, AVSim generates agent entities that accurately represent the population.

The movement of these agents is modeled using a novel probability-based approach informed by real-world GPS data collected from 100 individuals across various occupational classes. This innovative method effectively replicates human behavior and has been rigorously validated through an extensive study of human motion patterns.

Additionally, AVSim incorporates a realistic transport network, enabling agents to move via modeled transportation systems. It can simulate infections based on professional classes and supports a variety of analyses to study disease dynamics. Together, these capabilities place AVSim in a class of its own, far surpassing the limitations of other agent-based models.

The results from AVSim enable users to identify vulnerable agent groups and high-risk locations. Preventive measures, such as promoting safe hygiene practices and implementing vaccination campaigns, can then be simulated to assess their impact on mitigating disease spread. These simulations provide valuable insights, helping policymakers make informed decisions and implement strategies to control disease transmission while minimizing societal and economic disruption in the region.

## CRedit authorship contribution statement

**Pandula Thennakoon:** Writing – original draft, Data curation, Formal analysis, Methodology, Conceptualization. **Mario De Silva:** Writing – original draft, Data curation, Formal analysis, Methodology, Conceptualization. **M. Mahesha Viduranga:** Writing – original draft, Data curation, Formal analysis, Methodology, Conceptualization. **Sashini Liyanage:** Writing – original draft, Data curation, Formal analysis, Methodology, Conceptualization.



**Roshan Godaliyadda:** Conceptualization, Methodology, Supervision. **Mervyn Parakrama Ekanayake:** Conceptualization, Methodology, Supervision. **Vijitha Herath:** Conceptualization, Methodology, Supervision. **Anuruddhika Rathnayake:** Conceptualization, Supervision. **Ganga Thilakarathne:** Conceptualization, Supervision. **Janaka Ekanayake:** Conceptualization, Supervision. **Samath Dharmarathne:** Conceptualization, Supervision.

## References

- [1] COVID-19 deaths | WHO COVID-19 dashboard — data.who.int, <https://data.who.int/dashboards/covid19/deaths>, 2024. [Accessed 03-01-2025].
- [2] Vector-borne diseases — who.int, <https://www.who.int/news-room/fact-sheets/detail/vector-borne-diseases>, 2024. [Accessed 03-01-2025].
- [3] S. Gallagher, J. Baltimore, Comparing compartment and agent-based models, in: Joint statistical meeting, Baltimore, 2017, pp. 1–21.
- [4] S. He, Y. Peng, K. Sun, Seir modeling of the covid-19 and its dynamics, *Nonlinear Dynamics* 101 (2020) 1667–1680.
- [5] J. Dehning, J. Zierenberg, F. P. Spitzner, M. Wibral, J. P. Neto, M. Wilczek, V. Priesemann, Inferring change points in the spread of covid-19 reveals the effectiveness of interventions, *Science* 369 (2020) eabb9789.
- [6] G. Giordano, F. Blanchini, R. Bruno, P. Colaneri, A. Di Filippo, A. Di Matteo, M. Colaneri, Modelling the covid-19 epidemic and implementation of population-wide interventions in Italy, *Nature Medicine* 26 (2020) 855–860.
- [7] C. C. Kerr, R. M. Stuart, D. Mistry, R. G. Abeyesuriya, K. Rosenfeld, G. R. Hart, R. C. Núñez, J. A. Cohen, P. Selvaraj, B. Hagedorn, L. George, M. Jastrzębski, A. S. Izzo, G. Fowler, A. Palmer, D. Delport, N. Scott, S. L. Kelly, C. S. Bennette, B. G. Wagner, S. T. Chang, A. P. Oron, E. A. Wenger, J. Panovska-Griffiths, M. Famulare, D. J. Klein, Covasim: An agent-based model of covid-19 dynamics and interventions, *PLOS Computational Biology* 17 (2021) e1009149.
- [8] R. Hinch, W. J. M. Probert, A. Nurtay, M. Kendall, C. Wymant, M. Hall, K. Lythgoe, A. Bulas Cruz, L. Zhao, A. Stewart, L. Ferretti, D. Montero, J. Warren, N. Mather, M. Abueg, N. Wu, O. Legat, K. Bentley, T. Mead, K. Van-Vuuren, D. Feldner-Busztin, T. Ristori, A. Finkelstein, D. G. Bonsall, L. Abeler-Dörner, C. Fraser, Openabm-covid19—an agent-based model for non-pharmaceutical interventions against covid-19 including contact tracing, *PLOS Computational Biology* 17 (2021) e1009146.
- [9] F. F. Bastarion, T. O. Hancock, C. F. Choudhury, E. Manley, Agent-based models in urban transportation: review, challenges, and opportunities, *European Transport Research Review* 15 (2023).
- [10] R. L. Axtell, J. D. Farmer, Agent-based modeling in economics and finance: Past, present, and future, *Journal of Economic Literature* (2022) 1–101.
- [11] P. Maia, G. Pérez-Rodríguez, M. Pérez-Pérez, F. Fdez-Riverola, A. Lourenço, N. F. Azevedo, Application of agent-based modelling to assess single-molecule transport across the cell envelope of *e. coli*, *Computers in Biology and Medicine* 107 (2019) 218–226.
- [12] C. Borau, R. Chisholm, P. Richmond, D. Walker, An agent-based model for cell microenvironment simulation using flamegpu2, *Computers in Biology and Medicine* 179 (2024) 108831.
- [13] H. Weligampola, L. Ramanayake, Y. Ranasinghe, G. Ilangarathna, N. Senarath, B. Samarakoon, R. Godaliyadda, V. Herath, P. Ekanayake, J. Ekanayake, M. Maheswaran, S. Theminimulle, A. Rathnayake, S. Dharmaratne, M. Pinnawala, S. Yatigammana, G. Tilakaratne, Pandemic simulator: An agent-based framework with human behavior modeling for pandemic-impact assessment to build sustainable communities, *Sustainability* 15 (2023).
- [14] J. M. H. I. M. F. J. K. D. M. W. Carrie A. Manore, Kyle S. Hickmann, C. N. Mores, A network-patch methodology for adapting agent-based models for directly transmitted disease to mosquito-borne disease, *Journal of Biological Dynamics* 9 (2015) 52–72. PMID: 25648061.
- [15] I. Mahmood, M. Jahan, D. Groen, A. Javed, F. Shafait, An agent-based simulation of the spread of dengue fever, in: V. V. Krzhizhanovskaya, G. Závodszy, M. H. Lees, J. J. Dongarra, P. M. A. Sloot, S. Brissos, J. Teixeira (Eds.), *Computational Science – ICCS 2020*, Springer International Publishing, Cham, 2020, pp. 103–117.
- [16] F. Dayan, M. Rafiq, N. Ahmed, A. Raza, M. O. Ahmad, A dynamical study of a fuzzy epidemic model of mosquito-borne disease, *Computers in Biology and Medicine* 148 (2022) 105673.
- [17] A. Trivedi, N. K. Sreenivas, S. Rao, Modeling the spread and control of covid-19, *Systems* 9 (2021).
- [18] Q. Fan, Q. Li, Y. Chen, J. Tang, Modeling covid-19 spread using multi-agent simulation with small-world network approach, *BMC Public Health* 24 (2024) 672.
- [19] R. Hinch, W. J. M. Probert, A. Nurtay, M. Kendall, C. Wymant, M. Hall, K. Lythgoe, A. Bulas Cruz, L. Zhao, A. Stewart, L. Ferretti, D. Montero, J. Warren, N. Mather, M. Abueg, N. Wu, O. Legat, K. Bentley, T. Mead, K. Van-Vuuren, D. Feldner-Busztin, T. Ristori, A. Finkelstein, D. G. Bonsall, L. Abeler-Dörner, C. Fraser, Openabm-covid19—an agent-based model for non-pharmaceutical interventions against covid-19 including contact tracing, *PLOS Computational Biology* 17 (2021) 1–26.
- [20] P. Thennakoon, R. Rodrigo, K. Jayasooriya, T. Ragulakaran, R. Godaliyadda, V. Herath, M. P. Ekanayake, J. Ekanayake, Unveiling motion patterns through unsupervised clustering, in: 2024 6th International Conference on Advancements in Computing (ICAC), 2024, pp. 552–557. doi:10.1109/ICAC64487.2024.10851006.
- [21] S. Liyanage, M. Viduranga, M. De Silva, R. Godaliyadda, V. Herath, M. P. Ekanayake, J. Ekanayake, Real world data-driven agent-based modeling for health policy insights during epidemics, in: 2024 6th International Conference on Advancements in Computing (ICAC), 2024, pp. 546–551. doi:10.1109/ICAC64487.2024.10851169.
- [22] N. Nuraini, I. S. Fauzi, M. Fakhruddin, A. Sopaheluwakan, E. Soewono, Climate-based dengue model in Semarang, Indonesia: Predictions and descriptive analysis, *Infectious Disease Modelling* 6 (2021) 598–611.
- [23] T. A. Perkins, R. C. Reiner, G. España, Q. A. ten Bosch, A. Verma, K. A. Liebman, V. A. Paz-Soldan, J. P. Elder, A. C. Morrison, S. T. Stoddard, U. Kitron, G. M. Vazquez-Prokopec, T. W. Scott, D. L. Smith, An agent-based model of dengue virus transmission shows how multiple uncertainties about vaccine efficacy influence public health impact projections, *bioRxiv* (2018).
- [24] C. J. Dommar, R. Lowe, M. Robinson, X. Rodó, An agent-based model driven by tropical rainfall to understand the spatio-temporal heterogeneity of a chikungunya outbreak, *Acta Tropica* 129 (2014) 61–73. *Human Infectious Diseases and Environmental Changes*.
- [25] A. Kuzdeuov, A. Karabay, D. Baimukashev, B. Ibragimov, H. A. Varol, A particle-based covid-19 simulator with contact tracing and testing, *IEEE Open Journal of Engineering in Medicine and Biology* 2 (2021) 111–117.
- [26] A. Ebrahimi, Self-directed and self-designed learning: Integrating imperative topics in the case of covid-19, *Technologies* 11 (2023).
- [27] J. Gabler, T. Raabe, K. Roehrl, People meet people: A microlevel approach to predicting the effect of policies on the spread of covid-19, *SSRN Electronic Journal* (2020).
- [28] P. Mellacher, Covid-town: An integrated economic-epidemiological agent-based model, 2020. URL: <https://arxiv.org/abs/2011.06289>. arXiv:2011.06289.
- [29] M. S. Shamil, F. Farheen, N. Ibtehaz, I. M. Khan, M. S. Rahman, An agent-based modeling of covid-19: Validation, analysis, and recommendations, *Cognitive Computation* 16 (2021) 1723–1734.
- [30] H. Haddad, Z. Bouyahia, L. Horchani, On the sustainability of shared mobility since covid-19: From socially structured to social bubble vanpooling, *Sustainability* 14 (2022).
- [31] D. Birant, A. Kut, St-dbscan: An algorithm for clustering spatial-temporal data, *Data & Knowledge Engineering* 60 (2007) 208–221. *Intelligent Data Mining*.

- [32] M. Ester, H.-P. Kriegel, J. Sander, X. Xu, A density-based algorithm for discovering clusters in large spatial databases with noise, in: Proceedings of the Second International Conference on Knowledge Discovery and Data Mining, KDD'96, AAAI Press, 1996, p. 226–231.
- [33] F. R. Chung, Spectral graph theory, volume 92, American Mathematical Soc., 1997.
- [34] A. Y. Ng, M. I. Jordan, Y. Weiss, et al., On spectral clustering: Analysis and an algorithm, Advances in neural information processing systems 2 (2002) 849–856.
- [35] D. Y. L. Ranasinghe, H. K. Weerasooriya, S. Herath, M. P. B. Ekanayake, H. M. V. R. Herath, G. M. R. I. Godaliyadda, T. Madhujith, Transmittance multispectral imaging for reheated coconut oil differentiation, IEEE Access 10 (2022) 12530–12547.
- [36] D. Brockmann, Human mobility and spatial disease dynamics, Reviews of nonlinear dynamics and complexity 2 (2009) 1–24.
- [37] B. E. Cummings, C. N. Haas, L. J. Lo, C. M. Sales, J. Fox, M. S. Waring, Airborne disease transmission risks on public transit buses: Impacts of ridership, duration, and mechanical filtration using a relative risk metric, Building and Environment 255 (2024) 111303.
- [38] Dengue and severe dengue — who.int, <https://www.who.int/news-room/fact-sheets/detail/dengue-and-severe-dengue>, [Accessed 03-01-2025].
- [39] J. S. West, S. D. Atkins, J. Emberlin, B. D. L. Fitt, PCR to predict risk of airborne disease, Trends Microbiol. 16 (2008) 380–387.
- [40] N. S. Wong, S. S. Lee, K. M. Mitchell, E.-K. Yeoh, C. Wang, Impact of pre-event testing and quarantine on reducing the risk of COVID-19 epidemic rebound: a modelling study, BMC Infect. Dis. 22 (2022) 83.
- [41] C. B. Stauff, P. Selvaraj, F. D'Agnillo, C. A. Meseda, S. Liu, C. L. Pedro, K. Sangare, C. Z. Lien, J. P. Weir, M. F. Starost, T. T. Wang, Intranasal or airborne transmission-mediated delivery of an attenuated SARS-CoV-2 protects syrian hamsters against new variants, Nat. Commun. 14 (2023) 3393.
- [42] M. Soheili, S. Khateri, F. Moradpour, P. Mohammadzadeh, M. Zareie, S. M. M. Mortazavi, S. Manifar, H. G. Kohan, Y. Moradi, The efficacy and effectiveness of COVID-19 vaccines around the world: a mini-review and meta-analysis, Ann. Clin. Microbiol. Antimicrob. 22 (2023) 42.
- [43] F.-Z. Xiao, Y. Zhang, Y.-Q. Deng, S. He, H.-G. Xie, X.-N. Zhou, Y.-S. Yan, The effect of temperature on the extrinsic incubation period and infection rate of dengue virus serotype 2 infection in aedes albopictus, Arch Virol 159 (2014) 3053–3057.
- [44] G. Thennakoon, R. Rodrigo, K. P. Jayasooriya, R. Thiksga, M. C. L. De Silva, S. Liyanage, M. Viduranga, Spatio-temporal activity data across professional classes in Kandy, Sri lanka, 2024. doi:10.5281/zenodo.13621863.